NON-INVASIVE BEAM PROFILE MEASUREMENTS USING AN ELECTRON-BEAM SCANNER

W. Blokland, ORNL*, Oak Ridge, TN 37831, U.S.A.

Abstract

Two electron scanners, one for each plane, have been installed in the SNS (Spallation Neutron Source) Ring to measure the profile of the high intensity proton beam. The SNS Ring accumulates 0.6 μs long proton bunches up to 1.6e14 protons, with a typical peak current of over 50 Amp during a 1 ms cycle. The measurement is non-destructive and can be done during production. Electron guns with dipoles, deflectors, and quadrupoles scan pulsed electrons through the proton beam. The EM field of the protons changes the electrons' trajectory and projection on a fluorescent screen. Cameras acquire the projected curve and analysis software determines the actual profile of the bunch. Each scan lasts only 20 nsecs, which is much shorter than the proton bunch. Therefore the longitudinal profile of the proton bunch can be reconstructed from a series of scans made with varying delays. This talk will describe the theory, hardware and software of the electron scanner, as well as the results and progress made in improving the measurements.

INTRODUCTION

The electron scanner is a non-destructive alternative to a profile measurement instrument such as the wire-scanner. As such the electron scanner can run without restriction in regards to the beam intensity during neutron production. Electrons are accelerated up to 75 keV and scanned through the proton beam at a 45 degree angle, as shown in Fig. 1.

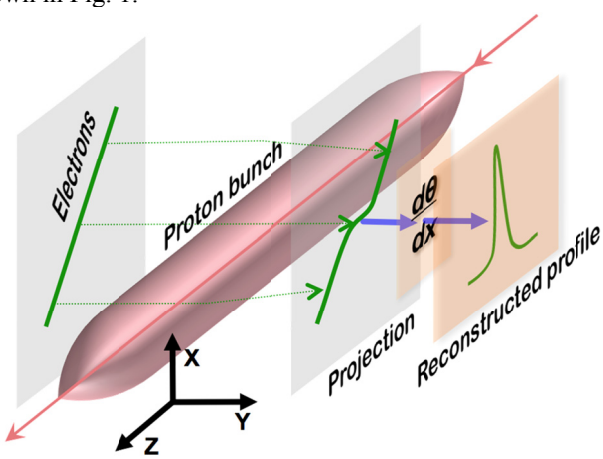

Figure 1: The deflection of the electrons.

The electron beam does not have to be tilted to derive the profile. However, the tilting makes the analysis easier and more accurate. For a vertical beam, the electrons are mostly deflected back on the same vertical trace and one must analyze the density distribution of the electrons along the vertical scan to derive the profile, see also [1]. Figure 2 shows simulated examples of both approaches. The figure shows the change in projection due to the deflection of the electrons for different beam widths "s" as well as the distribution density if the electron scan was vertically projected.

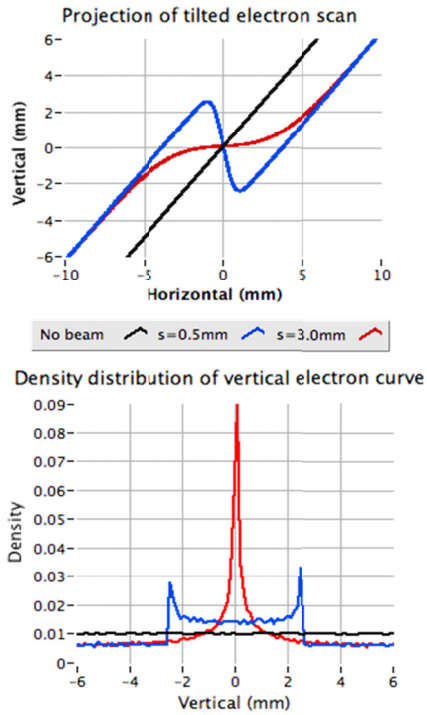

Figure 2: Simulation of the deflected electrons. The top figure shows the curve when scanned at 45 degrees, while the bottom figure shows the density distribution for a vertical scan.

By tilting the electron beam, the transverse profile can be derived from the angle of deflection of the electron beam passing by or through the proton beam. The derivation is shown in [2] and assumes that the path of the electrons is approximately straight, the net energy change to the electrons by the proton beam is close to zero, and the effect of the proton magnetic field can be neglected. The equation is as follows:

$$\frac{d\theta}{dx} = \int_L \frac{e}{mv^2} \cdot \frac{\delta(x,y)}{\varepsilon_0} dy$$

where e is the electron charge, m is the electron mass, v is the velocity, $\delta(x,y)$ is the proton beam density distribution, and θ is the electron beam deflection angle. Thus the profile is reconstructed by taking the derivative of the curve.

* ORNL/SNS is managed by UT-Battelle, LLC, for the U.S. Department of Energy under contract DE-AC05-00OR22725

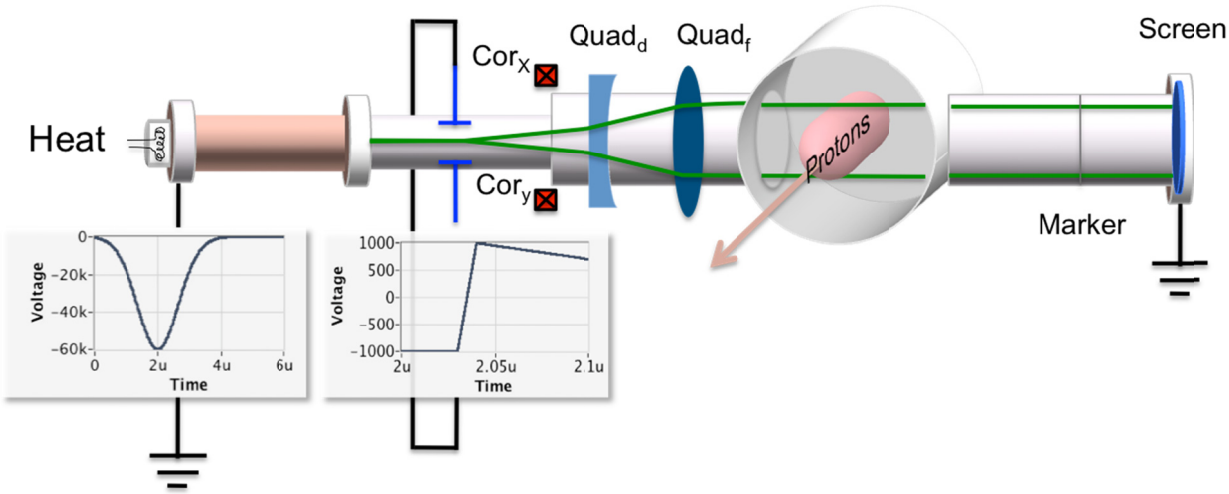

Figure 3: The layout of the Electron Scanner with the waveforms for the accelerating and deflector scan voltages.

ELECTRON SCANNER HARDWARE

The electron scanner, built by Budker Institute of Nuclear Physics (BINP) for SNS, is depicted in Fig. 3. The cathode is pulsed for about 1 µsec to about -65kV to accelerate the electrons. A deflector, oriented at 45 degrees, ramps in about 20 nsec to generate a diagonal scan. Two quadrupoles are used to increase the size of the scan and to produce a parallel path for the electrons within the scan. A horizontal and vertical corrector can adjust the position of the scan so it crosses the center of the fluorescent screen. Two markers slice a small part out of each side of the projected electron curve. The distance between the marker cutouts of the projection is the same as the distance between the actual markers if the electron scan was parallel and if there is no proton beam, see Fig. 4. The quads are adjusted until the distances are the same.

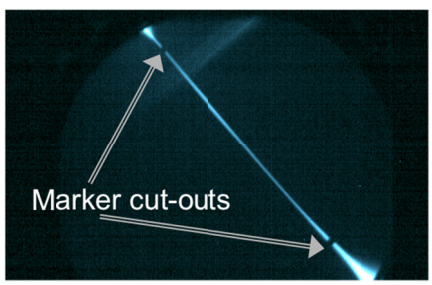

Figure 4: Projection of electrons with marker cut-outs.

Two scanners are installed in the Ring tunnel, one for the horizontal profile and one for the vertical profile. The horizontally mounted electron scanner, which produces the vertical proton beam profile, is shown in Fig. 5. Each scanner has a GigE Vision CMOS camera acquiring the images from the fluorescent screen. A PXI-based computer running LabVIEW controls the magnets, cameras, power supplies for the electron gun, and the deflectors.

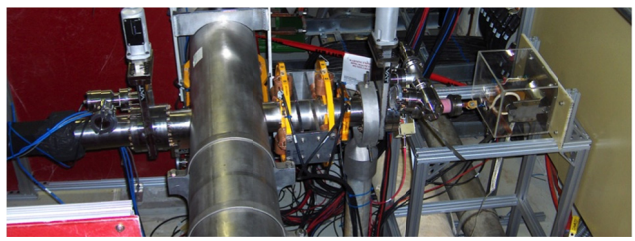

Figure 5: The horizontally mounted electron scanner.

ANALYSIS

The image of a typical scan for the horizontal profile with proton beam present is shown in Fig. 6. To calculate the profile from this curve, the derivative, *dy/dx*, must be taken.

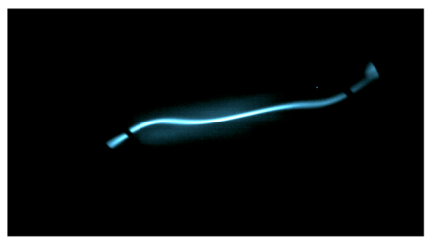

Figure 6: Electron projection for the horizontal profile affected by the proton beam.

First, the locations, a set of (x, y) points, of the curve is determined by finding the location, y, of the peak intensity in each column, x, of the image. This is done by either selecting the pixel in each column with the highest intensity or by fitting a Gaussian shape to the column intensity pixels and using the fitted centroid as the curve's location for that column. The later method is slower but produces better locations. The numerical derivative can be taken directly from the obtained locations, but this will give a very noisy profile. To reduce noise, a spline is fitted to the locations and then the derivative is taken from the fitted spline locations.

RESULTS

An example of a fitted spline is shown in Fig. 7. The spline can also pass over the marker cut-outs, extending the range of the profile to beyond the markers. This partially compensates for the too small aperture of the electron scanner for a typical production beam in the ring.

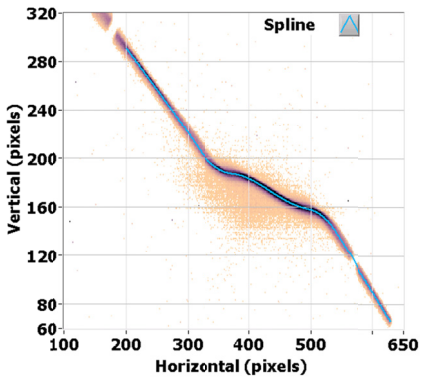

Figure 7: Overlay of the fitted spline (blue trace) with the image.

Because the scan duration of 20 nsec is short compared to the bunch length of 600nsec, the electron scanner can make multiple scans, offset by tens of nsecs, within the same bunch, see Fig. 8.

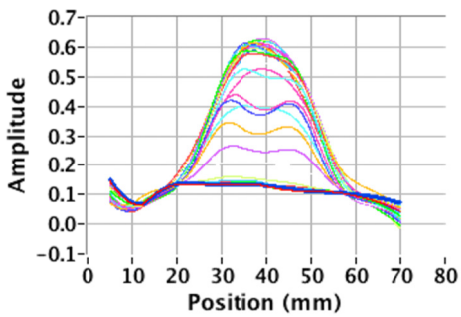

Figure 8: Horizontal profiles from multiple scans through the proton bunch in the same turn.

The multiple profiles of the same bunch can then be used to generate a composite image of a bunch that shows the longitudinal profile. Figure 9 shows the composite bunch shapes of the 10th, 20th, 30th, 40th, 50th, and 55th turn. Turns in between are left out of the plot to better show the accumulation of the beam in the Ring. Note that the projection of the bunch shape to the time axis equals a current monitor profile. The time scale increment is in 25nsec steps. The width is in pixels with approximate scale of 0.3 mm per pixel. Figure 10 shows a similar plot for the vertical profiles of the bunch for the different turns. It also shows that the vertical range of the electron scanner is not sufficient so that part of the profile is missing. While the vertical proton beam size can be adjusted by varying the vertical injection kicker, a smaller vertical size is not a typical production run setting.

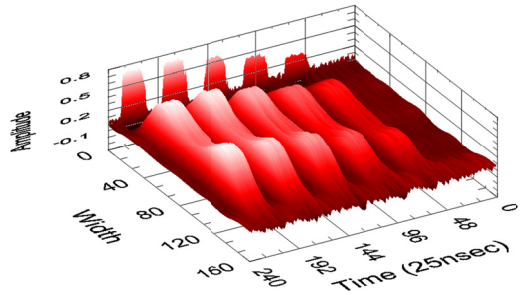

Figure 9: Composite plot of the horizontal profiles in turn 10,20,30,40,50, and 55.

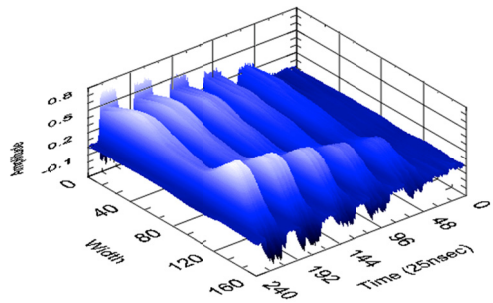

Figure 10: Composite plot of the vertical profiles in turn 10, 20, 30, 40, 50, and 55.

IMPROVEMENTS

Several improvements have been made to the electron scanner since its commissioning. Already discussed in [3] are improvements to the timing system and cameras.

Another issue was that the magnet stray fields affected the setup of the electron scanner and was also thought to distort the trajectory of the electrons other than just a linear translation. The main contributor was found to be the bus bar current for the Ring dipoles. For each different dipole current the electron scanner had to be retuned to position the trace within the fluorescent screen and to avoid electrons that do not fall within the scan from hitting the screen, see Fig. 11. After installing the magnet shielding, the jump in the projection diminishes significantly, no longer requiring any adjustments to the setup to correct for dipole or other magnet current changes.

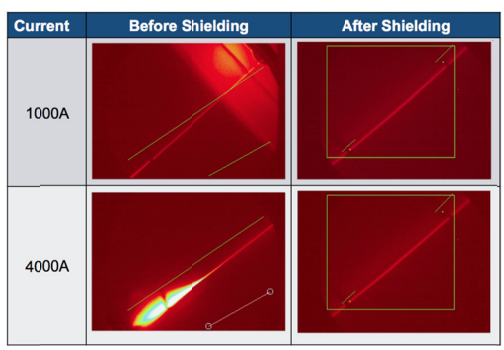

Figure 11: Effect of the ring dipole current on the electron scanner projection before and after shielding.

For certain setups, mostly lower proton beam intensities, a slope became apparent in the calculated profile, see Fig. 12. This slope in the profile makes the RMS calculation less accurate. Initially, it was thought to be mostly due to the stray external magnet fields. However, after shielding the electron scanner, the slope did not disappear from the profiles. Our current assumption is that this slope is due to the electron scan not going through the diagonal center of the quads and due to possible non-linearities in the quad fields. An initial calculation done by D. Malyutin from BINP showed that not going through the center of the quad could cause such a curvature. We are further investing this possibility, and in the meantime, modified the analysis to account for this curvature. This curvature shows up as a quadratic function in the trace on the image and as a slope in the profile.

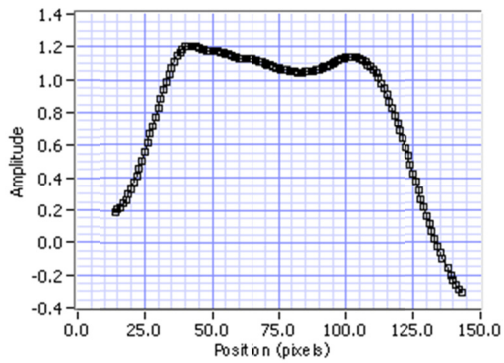

Figure 12: A visible slope in the calculated profile.

To adjust for the slope in the profile, the analysis fits a model of the expected beam profile plus the slope. The fitted function is then re-plotted with the slope removed.

The transverse beam profile in the SNS Ring differs significantly from the typical Gaussian function. Due to the injection scheme of beam into the ring and space charge effects, the profile often has a double peak. To model the double peak, two Gaussian functions can be used with one of the functions having an opposite amplitude and smaller sigma. This, however, does not quite account for the steepness of the slopes and, in the case of a single peak, the flatness of the peak. A better fit function, see [4] and [5], is the sum of two super-Gaussians with the same centroid:

$$f_{DSG}(x) = a_1 \cdot \exp\left(-\left(\frac{|x-\mu|}{\sigma_1}\right)^{n_1}\right) + a_2 \cdot \exp\left(-\left(\frac{|x-\mu|}{\sigma_2}\right)^{n_2}\right) + sl * x + o$$

where a_1 and a_2 are the amplitudes, μ is the centroid, n_1 and n_1 are the orders and σ_1 and σ_2 are the sigmas, sl is the slope, and o is the offset. By varying the order of the expression in the exponent, the flatness and steepness of the slope are adjusted, thus providing a better fit.

Figure 13 shows an example of the analysis process. The trace of red dots (raw) shows the, very noisy, profile as calculated from taking the derivative of the peaks for each column. The dark blue trace (spline) is the result of taking the derivative of the spline fitted to the peaks for each column. This is clearly much less noisy. The light blue trace (fit) is the double super-Gaussian with offset fitted to the spline. The green trace shows the fitted data with the slope removed. Other analysis methods are being investigated such as directly fitting the integral version of the double super-Gaussian to the curve in the image.

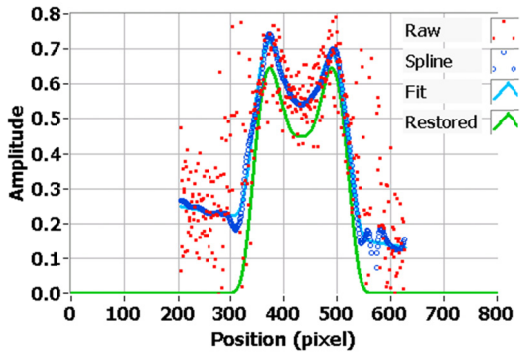

Figure 13: The removal of the slope from the fitted data.

COMPARISON

To compare the results of the electron scanner with an existing profile monitor, the RTBT (Ring to Target Beam Transfer line) harp, the harp profile was mapped back to the electron scanner location. The result agreed in terms of shape but disagreed by a factor of about 1.6 in terms of profile width. The beta functions used for this calculation are not well known and this could explain the difference. Efforts are underway to more accurately define the beta functions.

A second study bumped the proton beam at the electron scanner location to compare the BPM (Beam Position Monitor) measurements with the electron scanner measurements. Figure 14 is a superposition of the horizontal images of the electron projections of the orbit bumps and clearly reflects the movement of the proton beam.

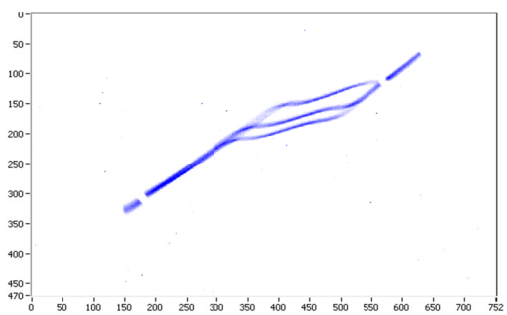

Figure 14: The superposition of three traces taken while bumping the orbit of the proton beam.

The analysis results for both planes are shown in Tables 1 and 2. These tables show the standard orbit and two bumps, one positive and one negative, as well as the corresponding jumps in measurement position by the electron scanner. The last row shows the sum of the

bumps and includes the estimated accuracies of the bump, ±0.5mm and the electron scanner measurement, ±0.5mm. It shows that the electron scanner is, at worst, off by about 15% horizontal and 10% vertical. The tables also show that for both planes the electron scanner must negate its direction to match with the BPM measurements.

Table 1: Results of Bumps in the Horizontal Orbit

Bump (mm)	ELS Pos (mm)	Difference (mm)	Error
- 7.0	66.7	+7.3	4%
0.0	59.4	0.0	NA
+ 3.4	55.6	-3.8	10%
Total Move (mm)	ELS Pos (mm)	Difference (mm)	Error
10.4±0.5		11.1±0.5	6±9 %

Table 2: Results of Bumps in the Vertical Orbit

Bump (mm)	ELS Pos (mm)	Difference (mm)	Error
- 5.0	68.2	+5.2	4%
0.0	63.4	0.0	NA
+ 8.0	55.3	-8.1	2%
Total Move (mm)	ELS Pos (mm)	Difference (mm)	Error
13.0±0.5		13.3±0.5	2±8%

SUMMARY

Additional improvements have been made to the operation of the electron scanner. Magnetic shielding has improved the ease of the setup. The analysis can now recover the profile despite the fact that the scan is not a straight line. The comparison with profiles in the RTBT and the comparison with the ring BPMs show that the electron scanner profiles obtained are reasonable. Further studies of the ring beta-functions are needed to confirm the correctness of the electron scanner profiles.

The capability to measure profiles of individual 20 nsec slices of beam anywhere along the 1 msec accumulation cycle is unique among the SNS diagnostic instrumentation.

FUTURE

To fully integrate the electron scanner into the accelerator operations, the setup and analysis must be fully automated. With the improvements made, we are now in the position to do just that. Work is in progress to automatically populate the initial estimates for the fitting routines. A table for all electron scanner magnet settings and accelerating voltage versus the proton beam charge will be created to automate the setup.

We plan to investigate the electron scanner's position jitter of 1mm peak-to-peak as well as install a lower jitter timing card to provide very repeatable measurements. In the long term we are looking to modify the vacuum chamber to widen the aperture and are investigating to use of electron scanners for tomography of the proton beam.

ACKNOWLEDGEMENTS

The author would like to acknowledge some of the many people who have worked on the electron scanner or helped taking data: S. Cousineau has done the comparison of the electron scanner profiles with the RTBT Harp profiles. T. Pelaia has setup the different orbits to perform the bump study. Without the work of S. Aleksandrov, D. Malyutin and S. Starostenko, the electron scanner wouldn't have been built.

REFERENCES

[1] E. Tsyganov, et al, "Electron beam emittance monitor for the SSC", Proc. PAC1993, pp.2489-2491.

[2] A. Aleksandrov et al, "Feasibility Study of Using an Electron Beam for Profile Measurements in the SNS Accumulator Ring", Proc. PAC 2005, pp. 2586-2588.

[3] W. Blokland et al, "Electron Scanner for SNS Ring Profile Measurements", Proc. DIPAC'09, Basel, Switzerland, 2009.

[4] F.-J. Decker, "Beam Distributions Beyond RMS", 6th Workshop on Beam Instrumentation, Vancouver, Canada, 3 - 6 Oct 1994, pp.550

[5] W. Blokland et al, "Fitting RTBT Beam Profiles: the case for the Super-Gaussian", Internal memo, SNS/RAD, ORNL, Nov, 2009.